Contribution from the School of Chemistry,
University of Western Australia, Nedlands, Australia 6009

Covalence in the $[Cr(CN)_6^{3-}]$ Ion Studied by X-ray Diffraction in $[Co(NH_3)_6][Cr(CN)_6]$ and $[Co(NH_3)_5(H_2O)][Cr(CN)_6]$

B. N. FIGGIS* and P. A. REYNOLDS

Received February 3, 1984

An X-ray diffraction experiment and structural refinement on $[Co(NH_3)_5(H_2O)][Cr(CN)_6]$ at 295 (1) and 120 (3) K show that it is isomorphous with the $R\bar{3}$ space group, $Z = 1$, structure of $[Co(NH_3)_6][Cr(CN)_6]$, with the water molecule equally disordered over the six ammonia sites; $R = 0.025$, $R_w = 0.033$ and $R = 0.026$, $R_w = 0.034$ at 295 and 120 K, respectively. The molecular geometry is as expected, but the larger size of the thermal parameters in the pentaammineaqua complex and their variation with temperature show the effect of disorder. The crystals were hexagonal prisms with $a = 0.7296$ (3) nm and $\alpha = 97.68$ (3)° at 120 K. The 120 K pentaammineaqua data and the preexisting hexaammine data at 80 K were refined with use of an aspherical valence electron population model. In spite of the differing thermal motion and crystal and experimental details, the derived valence electron parameters are closely similar. This agreement is an excellent test of the information that may be obtained from accurate X-ray data on transition-metal complexes. The $CN\cdots HNH_2$ hydrogen bonding appears to polarize the CN ligand π framework but has little effect on the σ framework. The metal atom electronic configurations are not significantly distorted from octahedral and show no evidence of long-range "intermolecular" effects on the metal atoms which occupy crystallographically trigonal sites. The metal configurations, $t_{2g}^{5.58(30)}e_g^{1.07(15)}$ and $t_{2g}^{2.66(30)}e_g^{1.07(15)}$ for Co and Cr, respectively, the observed metal–ligand overlap populations, 0.23 (4) and 0.15 (4), the CN σ electrons, and the ammonia lone-pair populations can all be analyzed in terms of a simple two-parameter-per-bond σ-bonding ligand field model, in which the ligands σ donate electrons into a bonding orbital involving only metal 3d orbitals. The lack of 4s or 4p populations contrasts with earlier work on M(II) complexes, reflecting the increased 3d–4s/p energy separation that is expected theoretically. The observed increased covalence of the M(III)–ligand bonds compared to those of M(II) is as expected, with Cr–CN being the most covalent. Although the data can be parameterized in a simple local, mainly σ-bonding, ligand field model, combination with other data, such as from spin density experiments, may well reveal the model to be inadequate, as in the earlier case of $Ni(NH_3)_4(NO_2)_2$. Comparison with theoretical calculations shows good agreement for the σ- and π-bonding parameters and metal configurations for both $Co(NH_3)_6^{3+}$ and $Cr(CN)_6^{3-}$. There may be, however, disagreement over the cyanide's internal electronic configuration, which reflects a neglect of $\sigma \rightarrow \pi^*$ configurations in the theoretical calculations, although our evidence is not statistically strong (2.3σ).

Introduction

The metal–cyanide bond is one of the most important for the understanding of covalency in metal–ligand bonding in transition-metal complexes. The cyanide ion lies high in the spectrochemical and nephelauxetic series of ligands,[1] leading us to expect a highly covalent metal–carbon bond. In addition it is a simple two-atom ligand and is believed to participate in both σ and π forms of bonding. It forms a well-known series of highly stable complex ions. By contrast with the position for the isoelectronic carbon monoxide molecule, in these series there are a number of cases with spin $S \geq {}^1/_2$.

This last-mentioned point invites a combined study of the charge density by X-ray diffraction and of the spin density by polarized neutron diffraction (PND). Of the available metal ions the most obvious one to consider is Cr(III), d^3, in the form of the hexacyano anion. For that ion the spin resides in bonding molecular orbitals in a simple MO description. The ground state is the orbitally nondegenerate $^4A_{1g}$ term, and that facilitates the interpretation of the PND data.

There is already available an excellent low-temperature X-ray diffraction data set on the compound $[Co(NH_3)_6][Cr(CN)_6]$.[2] Iwata has shown, using Fourier maps and least-squares valence population refinements, interesting covalent effects. As large single crystals are very difficult to grow, this compound is not suitable for the PND experiment.

In this paper we describe the preparation and structural study of the compound $[Co(NH_3)_5(H_2O)][Cr(CN)_6]$ (hereafter PAA) at 295 and at 120 K. We find this substance to be isomorphous with $[Co(NH_3)_6][Cr(CN)_6]$ (hereafter HA). Because of its higher solubility in water we have been able to grow large single crystals.

We subjected our 120 K PAA data and also Iwata's HA data[2] to the valence electron least-squares population analysis we have used successfully in other cases. The availability of two closely related data sets of high quality concerning the $Cr(CN)_6^{3-}$ ion probes the reproducibility of the results. We show, by means of Fourier maps, the sensitivity of our conclusions to the details of the least-squares modeling procedure. We also compare our conclusions on the HA complex with those of recent reanalysis of Iwata's data[3] and with theoretical calculations. The results of a PND experiment and an analysis of the spin density distribution in the $Cr(CN)_6^{3-}$ ion will be reported in due course.

Experimental Section

Well-faceted, purple pentaammineaquacobalt(III) hexacyanochromate(III) crystals, $[Co(NH_3)_5(H_2O)][Cr(CN)_6]$, were prepared by mixing equal volumes of carefully filtered 0.1 M solutions of $K_3Cr(CN)_6$ and $[Co(NH_3)_5(H_2O)](ClO_4)_3$.[4] Preliminary neutron diffraction results,[35] where H_2O and NH_3 contrast markedly, support the formula.

Specimens ~0.3 mm (120 K) and ~0.55 mm (295 K) in all dimensions were mounted on a Syntex $P2_1$ four-circle diffractometer equipped with a locally developed nitrogen gas cooled low-temperature attachment. Monochromatic Mo Kα radiation was employed. Data sets were collected at 295 (1) K and at 120 (3) K. In the following discussion we describe the 120 K data set, and in parentheses following, the 295 K set. The cell constants at 120 (295) K were determined by a least-squares refinement of the setting angles of 6 (6) reflections of the cell, indexed in the rhombohedral space groups $R3$ or $R\bar{3}$. A complete sphere of data was collected to a 2θ maximum of 50 (100)° and a hemisphere to 80 (−)°. The specification of standards, scan widths, and other parameters was as described previously.[5] No significant variation in the intensities of the standards was observed. The data were collected so that equivalent reflections were obtained at very different times. Crystal and experimental data are given in Table I. The data were corrected analytically for absorption with use of the program ABSCOR of the X-RAY 76 system.[6] The agreement factor between equivalents in the corresponding trigonal Laue symmetry was $R_I = \sum \mathrm{Av}(|I - \mathrm{Av}(I)|)/\sum \mathrm{Av}(I) = 0.023$ (0.023). The variances were estimated as described in our earlier work.[7] The value of $\sum\sigma(I)/\sum I$ was 0.015 (0.013), confirming the choice of rhombohedral space groups. Close inspection of the data failed to show any

(1) Jørgenson, C. K. "Absorption Spectra and Chemical Bonding in Complexes"; Pergamon Press: Oxford, 1962.
(2) Iwata, M. Acta Crystallogr. *Sect. B: Struct. Crystallogr. Cryst. Chem.* **1977**, *33B*, 59.
(3) Holladay, A.; Leung, P.; Coppens, P. *Acta Crystallogr., Sect. A: Found. Crystallogr.* **1983**, *39A*, 377.
(4) Jepson, C. A.; House, J. E. *J. Inorg. Nucl. Chem.* **1981**, *43*, 953.
(5) Figgis, B. N.; Reynolds, P. A.; Wright, S. *J. Am. Chem. Soc.* **1983**, *105*, 434.
(6) Stewart, J. M. "The X-RAY System-1976", Technical Report No. 446; Computer Science Center, University of Maryland: College Park, MD, 1976.
(7) Reynolds, P. A.; Figgis, B. N.; White, A. H. *Acta Crystallogr., Sect. B: Struct. Crystallogr. Cryst. Chem.* **1981**, *37B*, 508.

0020-1669/85/1324-1864$01.50/0

Table I. Crystal Data and Experimental Conditions for $[Co(NH_3)_5(H_2O)][Cr(CN)_6]$

	295 (1) K	120 (3) K
cryst dimens, mm (rhombohedral setting)		
$(11\bar{1})$ to $(\bar{1}\bar{1}1)$	0.52	0.30
$(10\bar{1})$ to $(\bar{1}0\bar{1})$	0.56	0.38
$(0\bar{1}1)$ to $(0\bar{1}\bar{1})$	0.56	0.30
$(\bar{1}10)$ to $(\bar{1}\bar{1}0)$	0.56	0.30
space group	$R\bar{3}, Z = 1$	
unit cell (rhombohedral setting)		
a, nm	0.7332 (2)	0.7296 (3)
α, deg	97.52 (2)	97.68 (3)
V, nm^3	0.3830 (2)	0.3769 (3)
unit cell (hexagonal setting)		
a, nm	1.1027 (3)	1.0986 (4)
c, nm	1.0912 (3)	1.0817 (4)
radiation	Mo K$\bar{\alpha}$ ($\bar{\lambda}$ = 71.069 pm)	
density, Mg m^{-3}		
measd	1.593 (5)	
calcd	1.604	
no. of measd reflcns	10 538	5298
no. of unique reflcns	2675	1573
$[(\sin\theta)/\lambda]_{max}$, nm^{-1}	10.80	9.07
μ(Mo K$\bar{\alpha}$), nm^{-1}	1.67	1.70
transmission factor	0.382–0.446	0.595–0.669

Table II. Rhombohedral to Hexagonal Parameter Transformation

hexagonal parameter	rhombohedral parameters
h	$h - k$
k	$k - l$
l	$h + k + l$
x	$^2/_3(2y - x - z)$
y	$^1/_3(x + y - 2z)$
z	$^1/_3(x + y + z)$
$U_{11}a^{*2}$	$a^{*2}(U_{11} + 4U_{22} + U_{33} - 4U_{12} + 2U_{13} - 4U_{23})$
$U_{22}a^{*2}$	$a^{*2}(U_{11} + U_{22} + 4U_{33} + 2U_{12} - 4U_{13} - 4U_{23})$
$U_{33}c^{*2}$	$a^{*2}(U_{11} + U_{22} + U_{33} + 2U_{12} + 2U_{13} + 2U_{23})$
$U_{12}a^{*2}$	$a^{*2}(-U_{11} + 2U_{22} + 2U_{33} + U_{12} + U_{13} - 5U_{23})$
$U_{13}a^*c^*$	$a^{*2}(-U_{11} + 2U_{22} - U_{33} + U_{12} - 2U_{13} + U_{23})$
$U_{23}a^*c^*$	$a^{*2}(U_{11} + U_{22} - 2U_{33} + 2U_{12} - U_{13} - U_{23})$

significant departure from the requirements of rhombohedral symmetry. Very long exposure photographs showed no evidence of supercell structure at 295 K, nor was highly correlated disorder indicated by streaking. For both PAA and HA we performed refinements of two types: first structural refinements to determine the atomic positional and thermal parameters, and second valence refinements to examine bonding effects in the charge density.

Structure

(a) Refinement. We performed refinements on the 120 and 295 K PAA data and, for comparison with our methods, on Iwata's 80 K HA data.[2] Initial coordinates were taken from the work of Iwata. In the space group $R\bar{3}$, with $Z = 1$, PAA must be disordered with the water molecule occupying equally the six "octahedral" Co(III) sites. Accordingly, for PAA we placed $^5/_6$ N plus $^1/_6$ O at each HA "N"(2) site. The quotes indicate the disordered nature of the site. With sufficient accuracy for an X-ray experiment, the two hydrogen atoms of the water molecule can be taken to be disordered over the three ammonia hydrogen sites in any occupation arrangement without symmetry constraint. Initially we assumed equal populations.

We performed these refinements in the rhombohedral setting. Since the rhombohedral to hexagonal parameter transformation is nonstandard[8] with the indexing used by Iwata and by ourselves, we list it in Table II. Least-squares refinements of atomic coordinates and anisotropic thermal parameters (for atoms other than H) was performed by employing the program CRYLSQ of the X-RAY 76 system[6] in the full-matrix mode. The function $\sum(\sigma(F_{obsd}))^{-2}(|F_{obsd}| - |F_{calcd}|)^2$ was minimized for those reflections with $I > 3\sigma(I)$. Neutral-atom scattering factors were used[9,10] and were modified, except for H, for anomalous dispersion.[11]

We obtained occupancies of 0.83 (8), 0.69 (7), and 0.89 (7) for H(1), H(2), and H(3), respectively, from the 120 K data set and at 295 K 1.12 (5), 0.85 (3), and 1.10 (3). The hydrogen atom occupancies are strongly correlated with the corresponding thermal parameter (coefficient ~0.8), as is usual in X-ray data analysis. The occupancy of H(2) is significantly lower than that of H(1) or H(3). We therefore adopted the assumption that the occupancies of H(1) and H(3) are unity, and that of H(2) is $^5/_6$, to account for the transition from $Co(NH_3)_6^{3+}$ to $Co(NH_3)_5(H_2O)^{3+}$. We point out that X-ray data is quite insensitive to hydrogen atom occupancies and the success of the above analysis of the disorder problem is better than would usually have been expected, emphasizing the quality of the data set. The subsequent neutron diffraction results on PAA[35] confirm this population analysis.

The refinement of the PAA 120 K data set with these hydrogen atom occupation constraints gave $R = 0.025$, $R_w = 0.025$ with 1127 "observed" reflections; at 295 K $R = 0.025$, $R_w = 0.033$ for 1769 data. There was no evidence of extinction. Reduction of the symmetry to $R3$ provided no significant improvement. HA (80 K)[2] gave $R = 0.026$, $R_w = 0.034$ for 2016 data. We define $R = \sum||F_{obsd}| - |F_{calcd}||/\sum|F_{obsd}|$ and $R_w = \sum\sigma(F_{obsd})^{-2}||F_{obsd}| - |F_{calcd}||/\sum\sigma(F_{obsd})^{-2}|F_{obsd}|$. These agreement factors appear sufficiently good that significant charge density information can be extracted from the data.

The structural and thermal parameters obtained from the preceding refinements are listed in Table III.

Table IIIA. Relative Coordinates ($\times 10^4$) and Isotropic Thermal Motion Parameters (pm^2), Given by $T = \exp(-8\pi^2\bar{U}(\sin^2\theta)/\lambda^2)$[a]

	x/a	y/b	z/c	$\bar{U}$
Co(1)	5000	5000	5000	57 (1)
	5000	5000	5000	142 (1)
	5000	5000	5000	231 (1)
Cr(1)	0	0	0	63 (1)
	0	0	0	158 (1)
	0	0	0	246 (1)
N(1)	2094 (1)	3894 (1)	−773 (1)	167 (3)
	2041 (1)	3935 (1)	−795 (1)	341 (6)
	2087 (1)	3883 (1)	−782 (1)	564 (5)
C(1)	1300 (1)	2502 (1)	−516 (1)	105 (2)
	1273 (1)	2544 (1)	−523 (1)	222 (5)
	1300 (1)	2510 (1)	−533 (1)	340 (3)
"N"(2)	6361 (1)	7333 (1)	4490 (1)	93 (2)
	6348 (2)	7332 (2)	4480 (2)	190 (5)
	6340 (1)	7320 (1)	4474 (1)	324 (3)
H(1)	7374 (27)	7169 (26)	4094 (26)	235 (44)
	7408 (21)	7230 (20)	4146 (20)	408 (42)
	7280 (20)	7227 (18)	4095 (18)	602 (40)
H(2)	6671 (25)	8140 (25)	5495 (25)	206 (42)
	6704 (24)	8197 (22)	5482 (25)	375 (50)
	6570 (24)	8182 (24)	5432 (25)	604 (48)
H(3)	5731 (28)	7792 (27)	3671 (29)	271 (47)
	5807 (20)	7771 (20)	3679 (20)	287 (38)
	5670 (20)	7759 (20)	3685 (20)	528 (36)

[a] The first entry for each atom is for HA at 80 K, the second for PAA at 120 K, and the third for PAA at 295 K.

(b) Molecular Geometry and Thermal Parameters. The ions in these salts are slightly trigonally distorted from body-centered cubic packing and are held together by a network of N–H···N hydrogen bonds.[2] The structure of HA has been fully discussed.[2] The interatomic distances and bond angles are listed in Table IV. The differences between Iwata's refinement and ours are small and are in the range expected from the different methods. The geometry of the $Cr(CN)_6^{3-}$ ion in PAA is entirely similar to that in HA. The C(1)–N(1) bond length in HA is 2 pm longer than in PAA and similar to that in other hexacyanochromate(III) anions.[12] In PAA the Co(1)–"N"(2) distances are 2 pm shorter than in HA. This presumably reflects the influence of the $^1/_6$ O atom at each "N"(2) site, since the Cr–O bond in $Cr(H_2O)_6^{3+}$ complexes is typically shorter than the Cr–N bond in complexes with the $Cr(NH_3)_6^{3+}$ ion.

In both HA and PAA the thermal motion does not decrease linearly with temperature. The ratio of the mean value of U_{ii}^2 at 80 and at 295 K is 0.38 (2) for the HA studies, compared with 0.27 (1) expected from the temperature ratio if the thermal motion is purely harmonic. For PAA

(8) "International Tables for X-ray Crystallography"; Kynoch Press: Birmingham, England, 1974; Vol. 1.
(9) Cromer, D. T.; Mann, J. B. *Acta Crystallogr., Sect. A: Cryst. Phys., Diffr., Theor. Gen. Crystalogr.* **1968**, *24A*, 321.
(10) Stewart, R. F.; Davidson, E. R.; Simpson, W. T. *J. Chem. Phys.* **1965**, *42*, 3175.
(11) Cromer, D. T.; Liberman, D. J. *J. Chem. Phys.* **1970**, *53*, 1891.
(12) Condon, E. U.; Shortley, G. H. "The Theory of Atomic Spectra"; Cambridge University Press: Cambridge, England, 1957.

Table IV. Interatomic Distances and Bond Angles[a]

	PAA		HA (80 K)	
	120 K	295 K	our refinement	Iwata (set B)
	Bond Lengths (pm)			
Cr(1)–C(1)	206.8 (1)	206.8 (1)	206.7 (1)	207.1 (7)
Co(1)–"N"(2)	195.7 (1)	196.0 (1)	197.8 (1)	198.0 (1)
C(1)–N(1)	114.7 (1)	114.1 (1)	116.2 (1)	115.7 (1)
"N"(2)–H(1)	85.1 (16)	78.4 (15)	85.6 (21)	85.3 (12)
"N"(2)–H(2)	88.5 (16)	86.4 (16)	86.6 (17)	86.0 (10)
"N"(2)–H(3)	78.9 (16)	83.3 (14)	84.5 (21)	85.9 (9)
	Bond Angles, deg			
C(1)–Cr(1)–C(1^{I})	90.30 (5)	90.08 (4)	90.15 (4)	90.15 (4)
"N"(2)–C(1)–"N"(2^{I})	89.54 (5)	89.59 (4)	89.45 (4)	89.54 (3)
Cr(1)–C(1)–N(1)	177.5 (2)	177.0 (3)	177.4 (2)	177.50 (5)
Co(1)–"N"(2)–H(1)	114.3 (10)	115.1 (10)	112.0 (13)	113.8 (8)
Co(1)–"N"(2)–H(2)	113.6 (12)	112.4 (12)	110.6 (13)	113.2 (7)
Co(1)–"N"(2)–H(3)	114.2 (9)	109.7 (9)	112.0 (13)	112.0 (6)
H(1)–"N"(2)–H(2)	99.6 (15)	107.7 (15)	106.1 (17)	104.8 (10)
H(1)–"N"(2)–H(3)	104.8 (16)	107.2 (14)	106.6 (20)	104.5 (10)
H(2)–"N"(2)–H(3)	109.2 (15)	104.1 (15)	109.4 (18)	108.0 (9)
	"N"(2)–H(3)···N(1^{II}) Bond			
"N"(2)···N(1^{II}), pm	293.0 (2)	295.2 (2)	297.8 (2)	297.5 (2)
H(3)···N(1^{II}), pm	216.0 (15)	212.8 (14)	214.6 (22)	213.2 (10)
"N"(2)–H(3)···"N"(2^{II}), deg	165.3 (15)	170.0 (16)	168.1 (20)	167.1 (9)

[a] Roman numeral superscripts indicate the following symmetry operations: I, z, x, y; II, $z, x, y-1$.

the respective ratios are 0.62 (5) and 0.41 (2). The departure from the harmonic approximation is obviously considerable, and the higher apparent "motion" at lower temperatures may be associated with the disorder of the water molecule in the cation. This disorder could cause the higher apparent thermal "motion" either by perturbing the interatomic distances in a random manner—a "static" mechanism—or moving between available sites—a "dynamic" mechanism. We cannot distinguish between the two mechanisms with the data presently available. The net effect is that at 120 K the thermal parameters of PAA are some 100% instead of 50% larger than those of HA at 80 K.

Valence Electron Density

(a) Theory and Model. To advance beyond a spherical atom treatment, we can use either an orbital[2,5] or multipole model[3] to describe the aspherical electron density. The two approaches can be identical if sufficient terms are used with the same radial functions. The metal sites (Cr and Co) are of sufficiently high symmetry ($\bar{3}$ or D_{3d}) that the data may support such an analysis.

The scattering from 3d electrons on a D_{3d} site can be completely described with five population parameters. We follow the methods of Condon and Shortley.[12]

We take the crystal c axis as the z quantization axis, and the x axis can be chosen arbitrarily. We choose this direction so that we can write the 3d atomic orbitals as

$$A_1 = |a_{1g}\rangle$$

$$E_2^+ = a|e_g^+(\pi)\rangle + \sqrt{1-a^2}|e_g^+(\sigma)\rangle$$

$$E_2^- = a|e_g^-(\pi)\rangle + \sqrt{1-a^2}|e_g^-(\sigma)\rangle \quad (1)$$

$$E_3^+ = \sqrt{1-a^2}|e_g^+(\pi)\rangle - a|e_g^+(\sigma)\rangle$$

$$E_3^- = \sqrt{1-a^2}|e_g^-(\pi)\rangle - a|e_g^-(\sigma)\rangle$$

where a is a mixing parameter dependent on the crystal field, and

$$|a_{1g}\rangle = d_{z^2}$$

$$|e_g^+(\pi)\rangle = \sqrt{2/3}d_{x^2-y^2} - \sqrt{1/3}d_{xz}$$

$$|e_g^-(\pi)\rangle = \sqrt{2/3}d_{xy} + \sqrt{1/3}d_{yz} \quad (2)$$

$$|e_g^+(\sigma)\rangle = \sqrt{1/3}d_{x^2-y^2} + \sqrt{2/3}d_{xz}$$

$$|e_g^-(\sigma)\rangle = \sqrt{1/3}d_{xy} - \sqrt{2/3}d_{yz}$$

In octahedral symmetry $e_g(\sigma)$ correlates with e_g, while $e_g(\pi)$ and a_{1g} correlate with t_{2g}. With orbital occupation numbers of p_1, p_2, and p_3 the electron density, ρ, can then be written

$$\rho = [p_1][\langle a_{1g}|a_{1g}\rangle] + [p_2a^2 + p_3(1-a^2)][\langle e_g^+(\pi)|e_g^+(\pi)\rangle + \langle e_g^-(\pi)|e_g^-(\pi)\rangle] + [p_2(1-a^2) + p_3a^2][\langle e_g^+(\sigma)|e_g^+(\sigma)\rangle + \langle e_g^-(\sigma)|e_g^-(\sigma)\rangle] + [2a\sqrt{1-a^2}(p_2-p_3)][\langle e_g^+(\pi)|e_g^+(\sigma)\rangle + \langle e_g^-(\pi)|e_g^-(\sigma)\rangle] \quad (3)$$

The scattering at wave vector $\vec{s}$ can be evaluated from this electron density by standard methods.[2,5,13] It involves four populations (first terms in brackets labeled as p_{A1}, $p_{E\pi}$, $p_{E\sigma}$, and $p_{\sigma\pi}$) and Fourier transforms of four overlap densities (second terms in brackets). The scattering factors for each of these second terms we label as

$$[\langle a_{1g}|a_{1g}\rangle]: \quad A1 = J_0 - 2.26476J_2 \text{ Re } (Y_2^0) + 3.038492J_4 \text{ Re } (Y_4^0)$$

$$[\langle e_g^+(\pi)|e_g^+(\pi)\rangle + \langle e_g^-(\pi)|e_g^-(\pi)\rangle]: \quad 2E\pi = 2(J_0 + 1.13238J_2 \text{ Re } (Y_2^0) - 0.33761J_4 \text{ Re } (Y_4^0) + 2.8246J_4 \text{ Re } (Y_4^3))$$

$$[\langle e_g^+(\sigma)|e_g^+(\sigma)\rangle + \langle e_g^-(\sigma)|e_g^-(\sigma)\rangle]: \quad 2E\sigma = 2(J_0 - 1.18163J_4 \text{ Re } (Y_4^0) - 2.82464J_4 \text{ Re } (Y_4^3))$$

$$[\langle e_g^+(\pi)|e_g^+(\sigma)\rangle + \langle e_g^-(\pi)|e_g^-(\sigma)\rangle]: \quad 2\sigma\pi = 2(1.6014J_2 \text{ Re } (Y_2^0) + 1.1936J_2 \text{ Re } (Y_4^0) - 0.9986J_4 \text{ Re } (Y_4^3))$$

J_N is defined by the equation $J_N = \int r^2[P_{3d}^2(r)]j_N(|\vec{s}|r)\,dr$, where $j_N(|\vec{s}|r)$ is the spherical Bessel function of order N, and $P_{3d}(r)$ is the radial part of the 3d atomic orbital. Re (Y_M^N) and Im (Y_M^N) are the real and imaginary parts, respectively, of the spherical harmonic Y_M^N.

If we chose the x axis of quantization as that naturally defined by the ligand atoms, then there is an extra scattering term

$$AX = 2J_4 \text{ Im } (Y_4^3) \quad (4)$$

with population P_{AX}. The angle θ_d between the x axis defined by the ligands and the axis allowing the wave function definition (1), i.e. the natural x quantization axis of the 3d orbitals, is given by

$$\theta_d = \tfrac{1}{3}\tan^{-1}[P_{AX}/[2.8246(P_{E\pi} - P_{E\sigma}) - 0.9986P_{\sigma\pi}]] \quad (5)$$

We can thus completely describe the scattering from a $\bar{3}$ site from 3d orbitals in three ways: (1) the five multipoles J_0, J_2 Re (Y_2^0), J_4 Re (Y_4^0), J_4 Re (Y_4^3), and J_4 Im (Y_4^3) and five associated populations; (2) The five scattering functions A1, Eπ, Eσ, $\sigma\pi$, and AX and five associated populations (P_{A1}, $P_{E\pi}$, $P_{E\sigma}$, $P_{\sigma\pi}$, P_{AX}); (3) The three sets of orbitals associated with the three populations (P_1–P_3) and the mixing parameter a (all defined by eq 1 and 2), together with the angle θ_d. The subscript on the population refers to the orbital numbering. The last description is the most physically transparent and is readily correlated with the octahedral case. There, with a d^3 ion as an example: $P_1 = P_2 = 1$, $P_3 = 0$, $a = 0$, $\theta_d = 0$ (case 3); $P_{A1} = 1$, $P_{E\pi} = 2$, $P_{E\sigma} = 0$, $P_{\sigma\pi} = 0$, $P_{AX} = 0$ (class 2). The multipole populations in this case are not necessarily even integral.

We have used the program ASRED,[13] which is written to produce the five populations p_{A1} to p_{AX} (case 2), because this gives a linear minimization. The physically more obvious parameters of case 3 must be derived from these.

Previous studies[13,14] have led us to expect that there may be some metal-centered charge density more diffuse than that of the 3d orbitals on each of the cobalt and chromium atoms and that this may be anisotropic in shape. Our modeling of the total valence charge distribution on the metal atoms consists of the five 3d-orbital populations and two 4p-orbital populations, $4p_z$ along the c axis and $4p_{x,y}$ ($4p_x = 4p_y$ by symmetry) perpendicular to it. Any 4s contribution would appear in the total 4p contribution. Associated with the respective orbital type was a radial parameter, κ_{3d} and κ_{4p}, such that the form factors were evaluated at $\kappa_{3d}\vec{s}$ or $\kappa_{4p}\vec{s}$ rather than at $\vec{s}$. There were, then, nine valence variables associated with each metal atom.

The C, N, and H sites are of such low symmetry that we have performed a restricted analysis for them because we are more interested in the metal atom and its bonding details than the CN^- and NH_3 fragments. On each atom in the ligands we placed s–p hybrid valence orbitals, chosen to correspond to the local bonding symmetry.[13-15] For the hydrogen

(13) Figgis, B. N.; Reynolds, P. A.; Williams, G. A. *J. Chem. Soc., Dalton Trans.* **1980**, 2339.
(14) (a) Chandler, G. S.; Figgis, B. N.; Phillips, R. A.; Reynolds, P. A.; Mason, R. *J. Phys. (Les Ulis, Fr.)* **1982**, *12*, C7-323. (b) Chandler, G. S.; Figgis, B. N. Phillips, R. A.; Reynolds, P. A.; Mason, R. *Proc. R. Soc. London, Ser. A* **1982**, *384*, 31. (c) Figgis, B. N.; Reynolds, P. A.; Mason, R. *Proc. R. Soc. London, Ser. A* **1982**, *384*, 49. (d) Figgis, B. N.; Williams, G. A.; Forsyth, J. B.; Mason, R. *J. Chem. Soc., Dalton Trans.* **1981**, 1837.

Table VA. Relative Coordinates ($\times 10^4$) and Isotropic Thermal Motion Parameters (pm^2) Derived by Refinement of High-Angle Data for PAA and HA Used in the Valence Refinement[a]

	x/a	y/b	z/c	$\bar{U}$
Co(1)	0	0	5000	145 (2)
	0	0	5000	59 (1)
Cr(1)	0	0	0	126 (2)
	0	0	0	56 (1)
N(1)	2206 (2)	2529 (2)	1734 (2)	330 (8)
	2156 (1)	2511 (1)	1741 (1)	150 (5)
C(1)	1443 (1)	1621 (1)	1095 (1)	214 (5)
	1402 (1)	1610 (1)	1093 (1)	101 (4)
"N"(2)	1281 (1)	1574 (1)	6056 (1)	169 (6)
	1275 (1)	1573 (1)	6063 (1)	379 (4)
H(1)	995 (18)	2092 (18)	6245 (16)	300 (77)
	962 (25)	2100 (25)	6262 (23)	169 (89)
H(2)	1405 (19)	1312 (21)	6722 (20)	134 (72)
	1389 (18)	1268 (19)	6790 (16)	−57 (48)
H(3)	1939 (19)	2046 (19)	5698 (17)	237 (71)
	2055 (22)	2010 (23)	5734 (22)	−27 (70)

[a] The first entry for each atom is for PAA at 120 K and the second for HA at 80 K. The hexagonal setting was used.

atoms modified H 1s functions were used.[10] On the nitrogen atoms ("N"(2)) of the ammonia molecules a $(sp^3)_\sigma$ tetrahedral set was employed with $(sp^3)_1$ directed toward the cobalt atom and the other three toward the hydrogen atoms. On the cyanide carbon and nitrogen atoms (C(1) and N(1)) sp hybrids were used, with $(sp)_1$ directed toward the chromium atom, together with a pair of π-type p orbitals, p_y and p_z, with axes such that y is perpendicular to c and x is parallel to the C(1)–Cr vector. Each non-hydrogen atom s–p hybrid set was given a radial parameter κ_{sp}. Each non-hydrogen ligand atom was thus associated with five variables. Contribution to the charge distribution by the "overlap" in the metal–ligand bonds was modeled by H 1s orbitals placed in the Co–"N"(2) and Cr–C(1) bond centers (OV(Co–"N"(2)), OV(Cr–C)). Together with the hydrogen atoms, which were treated individually, the model contained a total of 39 variables, including the scale factor.

The "core" and individual orbital form factors for the neutral atoms were employed and were taken from a standard compilation where available.[9-11,16] The Bessel function integrals, J_N, necessary for use with bond metal and ligand atoms were produced from the wave function,[17] by employing the local program JCALC, using the methods of Avery and Watson.[18]

Limits on the interpretation of the population parameters because of the projection of two-center terms into the one-center functions we employ, and of the radial parameters because of, for example, configuration interaction in the metal atoms, have been discussed.[5] The scale factor is a variable in this refinement. Errors in it and its correlation with the temperature factors in a normal refinement are partially corrected by appeal to electroneutrality on the crystal. We do this by a final rescaling of derived valence populations in order to put the populations on an absolute scale, rather than by use of electroneutrality as a constraint in the refinements, because it is a less biasing procedure. We can define a parameter, PR, as the necessary fraction to rescale the populations. While this parameter can be regarded as a measure of the projection efficiency of the model, we prefer to regard it as another empirical parameter that soaks up small errors, for example in the core form factors used or anharmonicity. Even for free atoms the difference between the usual single-configuration and multiconfiguration form factors for transition metals can be several percent.[19] This is aside from other effects (relativistic, covalence, crystal field, etc.) that may be present in our crystals.

(b) Refinement Procedure. The analysis of the data to obtain the valence electron distribution proceeded in the spirit of the *X–X* method. First, with use of the hexagonal setting, the data with $(\sin\theta)/\lambda > 7.0$ mm^{-1} was used in a conventional structural refinement for non-hydrogen atoms, based upon I_{obsd} with no data rejected, to give essentially "core" positional and thermal parameters listed in Table V for PAA. For HA

Table VI. Parameters Obtained in the Valence Refinements for PAA and HA Compounds for Spherical (S) and Aspherical (A) Treatments As Set Out in the Text

atom		PAA-S	PAA-A	HA-S	HA-A
Co	P_{A1}		2.08 (10)		1.98 (8)
	$P_{E\pi}$		3.78 (13)		3.31 (12)
	$P_{E\sigma}$		0.94 (17)		1.21 (13)
	P_{AX}		0.1 (9)		−0.6 (7)
	$P_{\sigma\pi}$		0.76 (24)		0.68 (16)
	$\sum P_{3d}$	6.87 (11)	6.79 (23)	6.47 (18)	6.50 (20)
	κ_{3d}	1.01 (1)	1.02 (1)	0.95 (2)	0.95 (2)
	$P_{4p_{x,y}}$		−1.0 (6)		−0.3 (5)
	P_{4p_z}		0.1 (3)		0.0 (5)
	$\sum P_p$	0.9 (10)	−0.9 (8)	1.5 (12)	−0.3 (8)
Cr	P_{A1}		0.98 (10)		0.88 (9)
	$P_{E\pi}$		1.40 (15)		2.07 (15)
	$P_{E\sigma}$		1.45 (14)		0.69 (14)
	P_{AX}		1.1 (8)		1.3 (7)
	$P_{\sigma\pi}$		0.38 (19)		0.38 (19)
	$\sum P_{3d}$	3.68 (13)	3.83 (23)	3.81 (28)	3.63 (22)
	κ_{3d}	0.90 (3)	0.97 (3)	0.84 (5)	0.84 (5)
	$P_{4p_{x,y}}$		0.3 (5)		0.5 (5)
	P_{4p_z}		0.1 (6)		0.1 (4)
	$\sum P_{4p}$	1.7 (9)	0.4 (9)	1.2 (11)	0.6 (8)
C(1)	$P_{(sp)_1}$		1.29 (10)		1.32 (11)
	$P_{(sp)_2}$		1.29 (12)		1.64 (19)
	P_{p_y}		0.84 (4)		0.78 (6)
	P_{pz}		0.76 (4)		0.54 (6)
	$\sum P_{(s,p)}$	3.91 (13)	4.18 (15)	3.95 (20)	4.29 (21)
	κ_{sp}	0.91 (4)	1.02 (3)	1.01 (5)	1.09 (3)
N(1)	$P_{(sp)_1}$		1.57 (9)		1.52 (15)
	$P_{(sp)_2}$		1.40 (4)		1.41 (6)
	P_{p_y}		1.62 (4)		1.54 (5)
	P_{p_z}		1.13 (4)		1.34 (5)
	$\sum P_{(s,p)}$	5.72 (9)	5.72 (11)	6.00 (13)	5.81 (16)
	κ_{sp}	1.12 (2)	1.13 (1)	1.33 (2)	1.31 (1)
"N"(2)	$P_{(sp^3)_1}$		1.44 (4)		1.45 (5)
	$P_{(sp^3)_2}$		1.22 (4)		1.16 (5)
	$P_{(sp^3)_3}$		1.26 (4)		1.23 (5)
	$P_{(sp^3)_4}$		1.23 (4)		1.30 (5)
	$\sum P_{(s,p)}$	5.29 (11)	5.16 (8)	5.03 (15)	5.13 (10)
	κ_{sp}	1.01 (1)	1.02 (1)	1.03 (1)	1.05 (1)
$\sum H$	$\sum P_H$	2.06 (8)	2.37 (8)	2.09 (8)	2.16 (7)
OV_{Co-N}		0.15 (4)	0.25 (3)	0.14 (6)	0.22 (5)
OV_{Cr-C}		0.18 (4)	0.14 (4)	0.14 (6)	0.15 (6)
PR		0.8690	0.8694	0.8543	0.8591
$R(I)$		0.046	0.047	0.044	0.038
$\chi(I)$		2.023	1.796	2.239	1.975
no. of observns		1573	1573	2058	2058
no. of variables		18	37	18	37

F_{obsd}^2 were used since the intensities were not available. The parameters changed little from those in the structural refinement. The parameters were then used, without being allowed to change, in the valence refinement using all the data, with a separate scale factor and with hydrogen positional and thermal parameters allowed to refine. The logic behind this procedure has been set out in connection with a previous example.[5]

In the first step the refinements were restricted to spherical atoms, thus forcing the metal 3d and 4p orbitals and the ligand s–p hybrid sets to be equally occupied in the sense of the full model. The radial parameters, κ_{nl}, were varied, as were the metal–ligand overlap "blobs". The refinements proved very insensitive to the radial parameters κ_{4p} for the metal atoms, and there was strong correlation with the corresponding population parameter. Accordingly, these 4p radial parameters were set at unity and not varied in the results quoted here. In other studies[14] where the data have supported the refinement of the metal κ_{4p} parameters, it has not been found to depart substantially from unity. Refinement continued until shift/error ratios did not exceed ca. 0.1. The results are presented as PAA-S and HA-S in Table VI.

Refinement then proceeded by allowing the various orbital population parameters to become unequal. The poor definition of the κ_{4p} parameters remained in this aspherical case, and they were retained as unity. The results are presented as PAA-A and HA-A in Table VI.

In these refinements we do not report the ammonia hydrogen atom populations separately, as, after correction for the $^5/_6$ occupancy of H(2) in the PAA case for the disordered water molecule, they do not differ within any one refinement by much more than the errors, which are typically 0.04 electron. In Figures 1 and 2 we show sections of the residual electron density in refinements PAA-S to HA-A including the

(15) Figgis, B. N.; Kucharski, E. S.; Williams, G. A. *J. Chem. Soc., Dalton* Trans. **1980**, 1515.
(16) "International Tables for X-ray Crystallography"; Kynoch Press: Birmingham, England, 1974; Vol. 4.
(17) Clementi, E.; Roetti, C. *At. Data Nucl. Data Tables* **1974**, *14*.
(18) Avery, J.; Watson, K. J. *Acta Crystallogr., Sect. A: Cryst. Phys., Diffr., Theor. Gen. Crystallogr.* **1977**, *33A*, 679.
(19) Barnes, L. A.; Chandler, G. S.; Figgis, B. N.; Glass, R.; Reynolds, P. A. *Acta Crystallogr., Sect. A: Found. Crystallogr.*, in press.

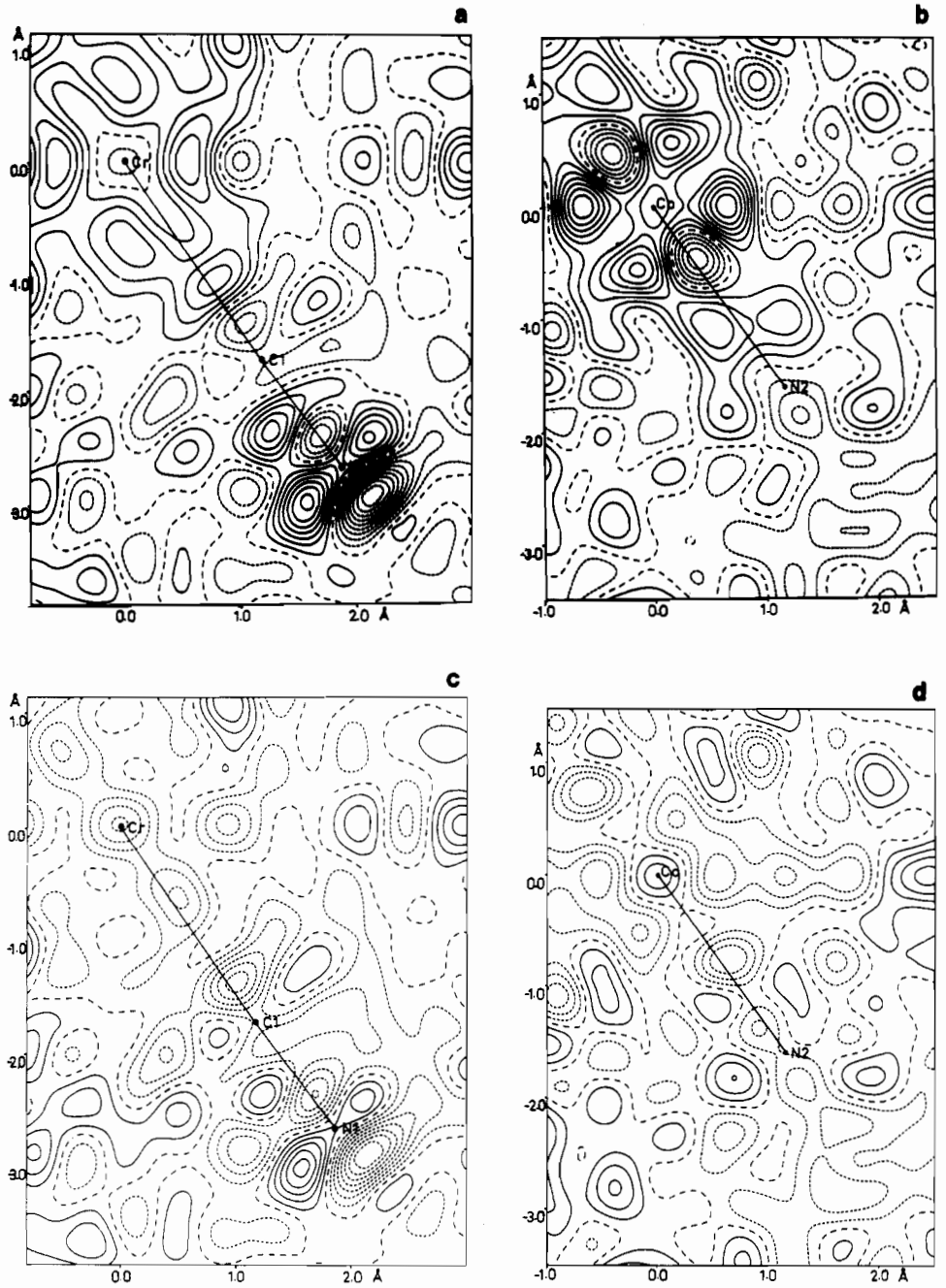

Figure 1. Residual densities for PAA (contour interval 100 e nm^{-3}; lines positive if solid, negative if dashed, zero if dotted; Co–Cr axis horizontal): (a) Co–Cr–CN plane, spherical atom refinement (PAA-S); (b) Cr–Co–"N"(2)(ammonia-*N*) plane, spherical atom refinement (PAA-S); (c) Co–Cr–CN plane, aspherical atom refinement (PAA-A); (d) Cr–Co–"N"(2) plane, aspherical atom refinement (PAA-A).

Co–Cr(3-fold) axis and the CN ligand and "N"(2), to illustrate respectively the Cr–CN bond and the Co"N"(2)(ammonia) bond. Apart from sections using refinements PAA-S to HA-A, we have also produced similar maps of the deformation density as the difference between the observed density and one using theoretical form factors (all $\kappa_{nl} = 1$). We used atomic positional and thermal parameters derived from high-angle data only and in a further series of maps those derived by use of all the data. In both cases the differences between these deformation densities and the residual densities of Figures 1 and 2 were very small. This is an encouraging sign of the robustness of our modeling.

It can be noted that a conventional multipole analysis[3] of the HA data based upon F_{obsd} produced the fit $R(F) = 0.0204$, $R_w(F) = 0.0219$, and $\chi(F) = 1.65$. We note that Holladay et al. constrain crystal electroneutrality and theoretical core populations (PR = 1) simultaneously. When we apply such a double constraint, e.g. to HA-S, while the goodness of fit changes insignificantly, the 4p populations become unphysically large and negative.

Results and Discussion

(a) Density Maps—Spherical Atom Model Residuals. (I) PAA. After subtraction of the spherical atom model density, Figure 1b shows the residual density in the Co–"N"(2) bond in the region of the cobalt atom. As in all these sections, the horizontal direction is the crystal threefold axis, the Co–Cr direction. Around the cobalt atom we see a pattern of peaks and holes, of magnitudes reaching 700 e nm^{-3} (0.7 e Å^{-3}) at about 60 pm, just as expected for low-spin Co(III) in a trigonal ligand environment approximating closely to octahedral symmetry, i.e. $a_{1g}^2e_g^4(\pi)e_g^0(\sigma)$ derived from $t_{2g}^6e_g^0$ in O_h. In addition, we see a substantial diffuse positive area peaking at 400 e nm^{-3} 80 pm from "N"(2) toward Co and this may be crudely interpreted as its lone pair. The Co–NH_3 bond features are, then, just as we might expect on a simple chemical basis.

In Figure 1a we see the corresponding Cr–CN density. Around the Cr atom there are again four peaks, two on the 3-fold axis of height 400 e nm^{-3} at 60 pm from Cr and two approximately where the maxima of the $e_g(\pi)$ orbitals should be, of height 300 e nm^{-3}, at 70 pm from Cr. The 2-fold reduction in height for this formally d^3 ion relative to the d^6 Co(III) case is as expected. Along the Cr–C(1) bond there is a hollow dipping to zero density and

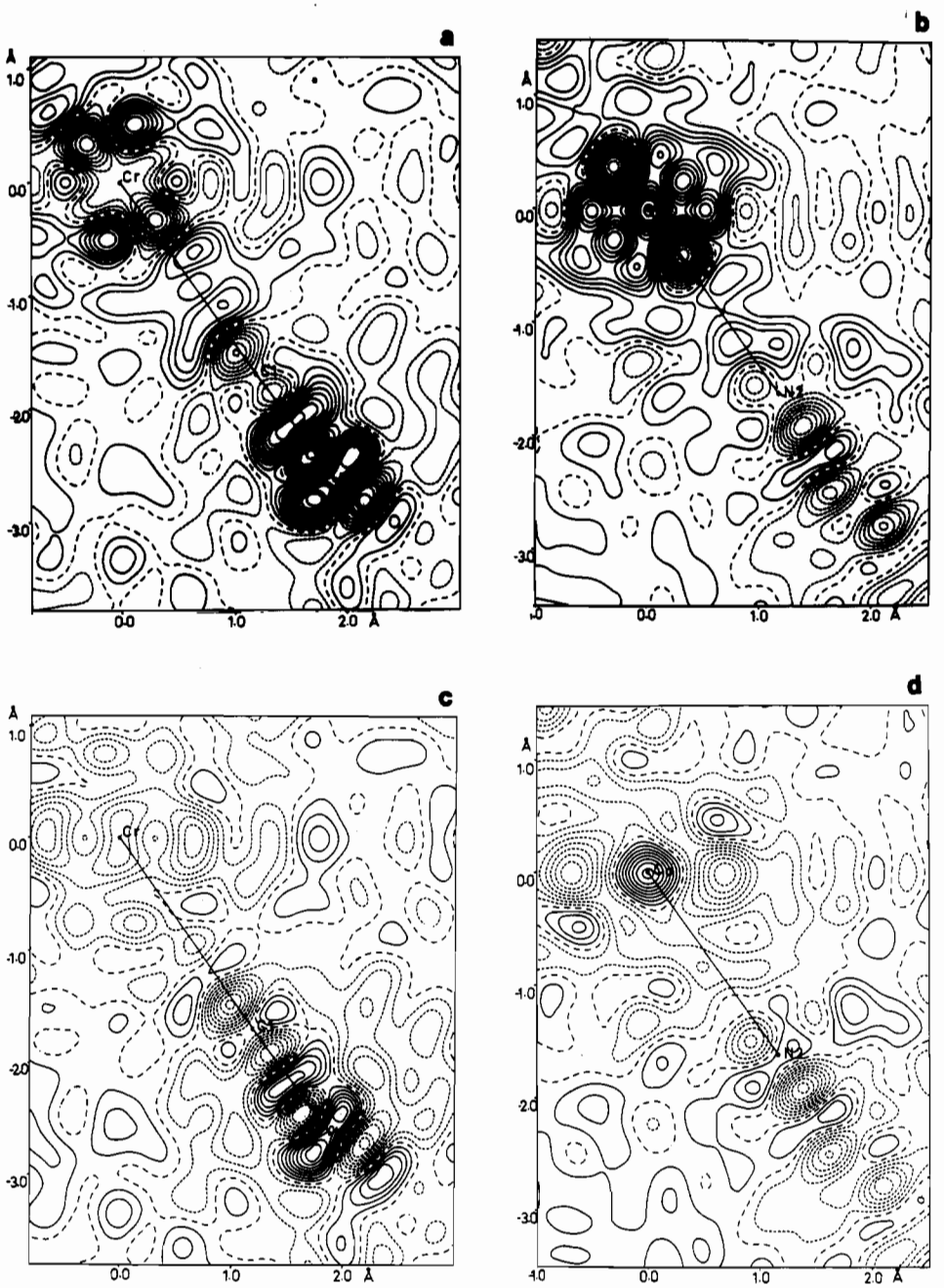

Figure 2. Residual densities for HA (contour interval 100 e nm^{-3}; lines positive if solid, negative if dashed, zero if dotted; Co–Cr axis horizontal): (a) Co–Cr–CN plane, spherical atom refinement (HA-S); (b) Cr–Co–N(2)(ammonia-*N*) plane, spherical atom refinement (HA-S); (c) Co–Cr–CN plane, aspherical atom refinement (HA-A); (d) Cr–Co–N(2) plane, aspherical atom refinement (HA-A).

located between the pair of "nonbonding" 3d peaks. The lack of an actual $e_g(\sigma)$ hole suggests an appreciable $e_g(\sigma)$ population, perhaps half that of the $e_g(\pi)$ orbitals. The Cr(III) configuration then appears to approximate to $a_{1g}^1e_g^2(\pi)e_g^1(\sigma)$, corresponding to an octahedral equivalent $t_{2g}^3e_g^1$, and there is some σ donation from CN^- into the 3d–$e_g(\sigma)$ orbitals. There is a peak (400 e nm^{-3}) approximately midway along the Cr–C(1) bond which reflects σ-bonding density derived from the C lone pair together with its overlap with the chromium atomic orbitals. Within the cyanide ion we observe very strong distortions from the spherical atom model, as might be expected from a formally triple bond. It does not resemble that observed for cyanide in $NaCN{\cdot}2H_2O$.[20] We postpone discussion of this until we treat the quantitative refinement.

(II) HA. Difference density maps for HA showing the same sections as for PAA are given in Figure 2a,b. Essentially the same maps have been presented and discussed by Iwata,[2] and here we restrict comment to comparison with those for PAA. In particular for the Co–N(2) bond around the cobalt atom we note four 900 e nm^{-3} peaks and two 1100 e nm^{-3} holes, corresponding to the $a_{1g}^2e_g^4(\pi)e_g^0(\sigma)$ configuration. A circular hole, 100 e nm^{-3} deep, lies between the a_{1g} and $e_g(\pi)$ peaks and might at first be confused with a further peak. There is a substantial residual density peaking at +1100 e nm^{-3} on the cobalt nucleus and a peak of 400 e nm^{-3} along the Co–N(2) bond at the N(2) lone-pair distance. In our HA maps, as partially shown also in Iwata's small displayed area, but not in the PAA maps, there are holes along the Co–N(2) direction, some 150 pm beyond N(2), which cannot be interpreted in terms of the N(2) atom electron density. These holes may be artifacts caused by errors or omissions in the data. The much lower thermal motion in HA, as well as raising 3d peak heights, also extends the observable range of intensities to higher values of 2θ. Additional peaks and troughs may arise if not all the observable data were collected. In the case of PAA all the observable data were collected.

(20) Bats, J. W. *Acta Crystallogr., Sect. B: Struct. Crystallogr. Cryst. Chem.* **1977**, *33B*, 446.

Table VII. Averaged Results for the Anisotropic Refinements over HA and PAA for Selected Populations[a]

		Co				Cr				
parameter	P_1	P_2	P_3	a	θ_D	P_1	P_2	P_3	a	θ_D
value	2.0 (1)	1.8 (2)	0.5 (2)	0.99 (1)	−1 (2)°	0.9 (1)	0.9 (2)	0.5 (2)	0.97 (3)	13 (8)
metal	unit	$Co_{t_{2g}}$	Co_{e_g}	Co_{4p}		$Cr_{t_{2g}}$	Cr_{e_g}	Cr_{4p}		
	pop./charge	5.58 (20)	1.08 (15)	−0.6 (6)		2.66 (20)	1.07 (30)	0.5 (5)		
ligand and	unit	"N"(2)$_{lone\ pr}$	$(NH_3)_{tot}$	$Co(NH_3)_6$		$C(1)_{lone\ pr}$	$N(1)_{lone\ pr}$	CN_π	$Cr(CN)_6$	
total	pop./charge	1.45 (4)	7.41 (20)	5.1 (6)		1.30 (10)	1.47 (2)	4.28 (10)	−5.1 (6)	

[a] The t_{2g} and e_g subscripts on metal populations show populations summed with neglect of deviations from octahedral symmetry.

In the Cr–C–N bond, as in the PAA results, there is lowering of Cr 3d peak heights compared to those of Co and a peak of about 500 e nm^{-3} midway along the Cr–C bond. The difference density in the CN bond region closely resembles that in the PAA case. The higher peaks and deeper troughs result from the smaller thermal smearing in the HA data.

Our overall conclusions from examining the difference density maps are as follows: (i) Given the different effective thermal motion parameters, the maps for HA and PAA are entirely similar. (ii) The features around the metal atoms and in the metal–donor atom bonds seem to conform to a classical chemical description of the bonding, such as we use as a basis for the modeling in the ASRED program. (iii) The electron distribution in the CN triple bond is complex. Simple hybrid orbital models are unlikely to describe it well.[21]

(b) Density Maps—Aspherical Atom Model Residuals. The residual maps of the difference between the observed and the model aspherical difference maps all show similar features and are discussed collectively. The "aspherical residuals" (Figures 1c,d and 2c,d) are directly comparable with the spherical model difference densities (Figures 1a,b and 2a,b, respectively).

We note a substantial reduction in density around both Co and Cr in both compounds, indicating that the aspherical 3d densities of the model form a good representation. The residual features are approximately half the magnitude of those using the spherical model. They are not always clear but are mainly holes 50–100 pm from the metal and either crystal c or the bond axes (Co–"N"(2), Cr–C). This indicates that the valence density close to both metal atoms is not accurately described by 3d orbitals with a single radial function. Various theoretical explanations in terms of "differential" nephelauxetic effects, "4d participation", or differing mixtures of basis functions in ab initio calculations are well-known, so this observation causes little surprise.

In the mid-bond region the "overlap" function and the atom-centered aspherical functions have been satisfactorily modeled.

The strong features observed in the cyanide in both data sets, and to a much lesser extent in the ammonia molecule, are *not* well modeled by our aspherical functions as expected from previous theoretical studies.[21] However, the total atomic populations we quote are unlikely to be grossly in error given the low correlation observed in this and our other studies between the various orders of multipole.

(c) Comparison of Different Refinements. In Table VI we see that the spherical and aspherical refinements do not disagree significantly for a given compound except, possibly, that for both metal atoms and compounds the 4p population is distinctly less for the aspherical refinements than the spherical refinements. Although this is significant only at the 2σ level for individual parameters, over the four parameters the reduction of the mean 4p population is probably meaningful.

One of the more important and encouraging conclusions of this whole study, at a practical level, is the generally excellent agreement between the HA-A and PAA-A refinements. From a chemical viewpoint the two compounds are expected to be so similar that any substantial disagreement would have thrown doubt onto the whole X-ray diffraction experiment and analysis as a method of establishing charge density distributions. This quantitative agreement occurs in spite of the much higher thermal parameters for PAA, whose effects were obvious in the residual density maps. The PAA parameter least-squares errors are comparable with those of HA in spite of the larger thermal motion. Although one reason could be better quality of the PAA data, it is more probable that, providing that the thermal motion is small enouth not to smear the valence density unduly, its actual size is not very important. This implies Tr (U_{ii}) of less than about 200 pm^2 for each atom. We also note that the esd's indicate that the water molecule disorder has been adequately described and modeled. A small residual effect of the disorder may be the larger κ_{3d}'s for PAA-A than HA-A; however, the same effect is not visible in κ_{sp}("N"(2)), where one might expect it. The only large discrepancy is in the κ_{sp}(N(1)) values, which differ by more than 10σ. The values of 1.13 (1) and 1.31 (1) are both markedly greater than the free-atom value of 1.0. This is probably a reflection of the marked bonding effects in the C≡N$^-$ ion, which are visible as strong features in the density maps. The discrepancy may result from either inadequacy of the s–p hybrid model and/or the larger thermal motion for the end atom (N(1)), especially in PAA-A.

Because of the excellent agreement of the four refinements we will restrict our discussion of the results to an average of PAA-A and HA-A. In Table VII we list some pertinent results of the refinements (PAA-A/2 + HA-A/2).

(d) Comparison with Previous Work. For the HA data there have been two previous analyses.[2,3] Iwata's analysis was essentially a spherical model refinement on F^2. Holladay et al.[3] used a multipole refinement on F_{obsd} with 68 variables on 2042 (sic) data. The weighting schemes also differ slightly from ours. Both Iwata and Holladay et al. apply an electroneutrality constraint during the refinement, unlike our procedure. There are also other small differences, such as Iwata's method of refinement for hydrogen atoms.

For the nonmetal atoms Iwata's spherical results generally agree well with our charges and radial expansions (note κ(Iwata) $\simeq 1/\kappa$(present work)). However, for the metal atoms there is significant disagreement. The results of Holladay et al. are closer to ours and include aspherical populations. For Co we obtained $3d^{6.65(20)}$ $(a_{1g}{}^{2.03(9)}e_g(\pi)^{3.54(20)}e_g(\sigma)^{1.07(20)})$, Iwata obtains $3d^{8.94(8)}$, and Holladay et al. obtain $3d^{7.84(9)}$ $(a_{1g}{}^{2.06}e_g(\pi)^{3.88}e_g(\sigma)^{1.88})$. For Cr we obtain $3d^{3.73(20)}$ $(a_{1g}{}^{0.93(10)}e_g(\pi)^{1.73(30)}e_g(\sigma)^{1.07(30)})$, Iwata obtains $3d^{5.36(9)}$, and Holladay et al. obtain $3d^{5.26}$ $(a_{1g}{}^{1.02}e_g(\pi)^{2.62}e_g(\sigma)^{1.61})$.

It is evident that the disagreement is systematic. Our 3d populations are less than those of Holladay et al., which in turn are less than Iwata's. The difference between the first two arises almost solely from the $e_g(\sigma)$ populations. It is our experience with this and other systems[5,14,22] that the spherical term, i.e. the total 3d population, is the most important in the fit. If this is fixed well away from its minimum value, then the aspherical terms are grossly affected in unpredictable and unphysical ways. The 3d populations of Iwata thus seem to be "fixed" away from the minimum, with Holladay's less so. We believe that this is a biasing effect of the electroneutrality constraint. Application of such a constraint with refinement on F^2(Iwata) forces a fit to the low-angle reflections, which have higher $\overline{F^2}$ values than medium-angle reflections. If electroneutrality is constrained and refinement is

(21) (a) Bats, J. W.; Feil, D. *Chem. Phys.* **1977**, *22*, 175. (b) Bats, J. W.; Feil, D. *Chem. Phys. Lett.* **1977**, *26*, 79.

(22) Figgis, B. N.; Reynolds, P. A.; Mason, R. *J. Am. Chem. Soc.* **1983**, *105*, 440.

on F(Holladay et al.), the bias toward lower angle is less, since the variation of $\bar{F}$ with $(\sin\theta)/\lambda$ is less than for $\overline{F^2}$. Our lack of electroneutrality constraint in the refinement allows the 3d populations to get to the deepest minimum the data permit, while PR deviates substantially from unity (to about 0.9). The application of an electroneutrality constraint in the refinement presupposes that the core electrons have been dealt with correctly—for example that the form factors are accurately known, that anharmonicity is negligible, and that TDS is well-behaved. In systems where the scale factor has been measured directly, there are often differences of up to 10% from the value estimated by structural refinement.[23] The origin of the difference is not known, and it seems to us overconfident to apply an electroneutrality constraint during refinement since a priori argument shows that this will be more biasing, if the scale factor and possibly other parameters are significantly in error, than correction after the refinement.

(e) Net Charge Transfers and Hydrogen Bonding. Table VII presents two possibly disturbing features—net complex ion charges of 5.1 (6)± for $Co(NH_3)_6$ and $Cr(CN)_6$, and a net charge of 1.0 (2)− on the cyanide group. Taken together, these indicate that we cannot regard the complex ions as independent entities of charge 3± within which σ and π bonding occur to give a CN charge >1−. It is possible that the hydrogen bonding "N"(2)–H···N(1)–C(1) has a noticeable effect on the charge distribution. The average hydrogen population, 0.73 (2), is well-defined in this study, reflecting the quality of the data set and the simplicity of the crystal structure. The low apparent H atom charges are the result of the large N–H overlap population, and the effect is well understood.[24] The equality of the occupation-corrected populations of H(1), H(2), and H(3) encourages confidence in other aspects of the population analysis. Any difference would have had to be ascribed to differential hydrogen bonding. In $Ni(NH_3)_4(NO_2)_2$, where this *does* occur, the population differences in crystallographically inequivalent hydrogens are also reflected in other properties, such as N–H stretching frequencies. Here, for example, the N–H stretches are observed to all lie in the normal ($\sim$3000 cm^{-1}) region, indicating no large differences in bonding between inequivalent hydrogens. With the model we employ it may be that a division of electron density into $Cr(CN)_6$ and $Co(NH_3)_6$ units cannot be made properly because significant electron density is transferred from the "N"(2)–H bond regions to the H···N(1) hydrogen-bonding region. The H···N(1) hydrogen-bonding density is arbitrarily divided in our simple model, with the bulk ending up as N(1) and thus giving a complex ion charge of less than 3− and a CN charge of about 1− in the $Cr(CN)_6$ ion.

(f) "Intermolecular" vs. Ligand Effects on Metal Bonding. Before proceeding we enquire whether there is any evidence of "intermolecular" effects on the metal–ligand bonding. By "intermolecular" we mean influence from the crystal region outside a complex ion, as distinct from the "ligand field" effects of the nearest neighbor coordinated ligands. The "intermolecular" term may or may not mean a direct electrostatic influence. Indeed, as the PND experiment on $Ni(NH_3)_4(NO_2)_2$ showed, the hydrogen bonding can transmit long-range effects that are observable in the spin density distribution.[22] The coordinated ligands lie very close indeed to the ideal octahedral positions around the metal atoms. Experience with theoretical calculations shows that such small distortion should give negligible departure from octahedral symmetry in the metal atom electronic structure. Evidence of $\bar{3}$ symmetry in the metal atom populations would reflect the longer range "intermolecular" effect.

Lowering of the metal atom site symmetry would induce mixing of $e_g(\sigma)$ and $e_g(\pi)$ to give a value of a, the mixing parameter, significantly different from unity. The values of 0.99 (1) and 0.97 (3) for Co and Cr respectively imply no significant mixing. The symmetry lowering might also cause the a_{1g} and $e_g(\pi)$ population parameters (P_1 and P_2) to differ. Although the a_{1g} population is larger for both Co and Cr, the difference is not significant at the 2σ level.

A third symptom of the long-range effects could be a rotation of the 3d quantization axes away from the directions defined by the ligands. The relevant angle, θ_d, is not significantly different from zero.

On all three grounds the esd's are sufficiently small that long-range low-symmetry effects are unlikely to be important in comparison with the local ligand effects. To the extent that long-range interactions produce octahedral symmetry effects on the metal atoms, they are part of the "ligand field".

(g) The Metal-Ligand Bonds, Ligand Field Theory, and Covalence. Given the absence in the Fourier maps of observed long-range influence on the metal–ligand bond region, we attempt a description of the Co–NH_3 and Cr–CN bonds in terms of simple ligand field theory. Our earlier studies on $Ni(NH_3)_4(NO_2)_2$[5,22] showed an ordinary ligand field model to be qualitatively correct, but grossly in error quantitatively, especially when the PND (spin density) and X-ray diffraction (charge density) results were considered together.

(I) Metal Atom and Overlap Regions. According to our modeling, Co resembles a free ion: the net charge is about 2.9+ with little significant population of 4p (−0.6 (6)) electrons. Cr has a lower net charge, about 1.8+, and again 4p contributions are hardly significant (0.5 (5)). The lack of 4p occupation is in contrast to our studies on M(II) ions,[5,14,22] where we found the total metal charge to be closer to 0 than to 2+, the dominant cause being relatively large 4s or 4p populations. In the present case, while for both Cr and Co there appears to be a σ donation of 1.1 (3) and 1.1 (2) *into* the metal 3d orbitals, the lack of 4p participation leaves the net metal charge closer to 3+ than 0. 3d to 4s/4p energy separations are known to be greater in M(III) compared to M(II) ions, and this may be the reason that 4s/4p populations appear to be so drastically reduced. The 4s/4p populations may be very sensitive to the "oxidation state" of the metal ion within the complex. The movement of density into the 3d orbitals is expected if σ donation from ligands is the major covalent effect. The small positive overlap populations in both the Cr–C and Co–N(2) bonds of 0.15 (4) and 0.24 (4) electron are also consistent with bonding involving metal 3d and ligand orbitals, where the ligands donate four electrons to form two bonding molecular orbitals. Since the electrons are in *bonding* orbitals, we expect a net accumulation of overlap electronic density. We contrast this with $Ni(NH_3)_4(NO_2)_2$, where two bonding orbitals *and* one antibonding orbital are occupied. For reasons connected with orthonormality, the antibonding *depletion* of overlap density per orbital is greater than the bonding orbital accumulation.[22] The net effect is the observation and prediction, in that case, of no significant overlap density even though there is strong covalent bonding.

The effect of metal–ligand bonding on the ligands may be complicated by their simultaneous participation in the H_2N–H···NC hydrogen bonds. Since the metal–ligand and hydrogen bonds involve different ends of the ammonia and cyanide molecules and different geometries, it may be possible to separate their effects by the differing influences on the charge balance within the molecules and the charge asphericity on the atoms. We therefore interpret the asphericity on the metal atoms, and the covalent region in terms of a simple ligand field theory, given the small effect that hydrogen bonding seems to have on this region.

The balance of π and σ metal–ligand bonds is, in this simple model, given by the populations $P_{A1} + P_{E\pi}$ and $P_{E\sigma}$. For Co we have 5.58, (20) π and 1.07 (15) σ, while for Cr we have 2.66 (20) π and 1.07 (30) σ. We see that the main change from the crystal field–no-covalence configurations of $6\pi + 0\sigma$ and $3\pi + 0\sigma$ for Co and Cr, respectively, consists of a gain, in both cases, of about 1.07 electrons in the σ-bonding orbitals. The π populations are slightly reduced. Thus, as would be predicted by the most elementary picture of covalence in the complex ion, the σ donation into the empty metal $3d_\sigma$ orbitals is substantial, while the π interaction has produced a possible depletion in the metal π orbital,

(23) Stevens, E. D.; Coppens, P. *Acta Crystallogr., Sect. A: Cryst. Phys., Diffr., Theor. Gen. Crystallogr.* **1975**, *31A*, 612.
(24) Olovsson, I.; Jonson, P. G. "The Hydrogen Bond"; Schuster, G., Zandel, G., Sandorfy, C., Eds.; North-Holland: Amsterdam, 1976; p 393.

Table VIII. Experimental and Theoretical Results for Some Significant Bonding Parameters in $Cr(CN)_6^{3-}$ and CN^-

		$Cr(CN)_6^{3-}$		CN^-		$NaCN\cdot 2H_2O$
	this experiment	ab initio[32]	$X\alpha$[33]	ab initio[34]	$X\alpha$[33]	expt[20]
d_π pop.	2.66 (20)	2.97	2.88			
d_σ pop.	1.07 (30)	0.81	1.28			
4s/4p pop.	0.5 (5)	0.63	0.62			
metal charge	1.8 (5)+	1.7+	1.2+			
C σ pop.	4.77 (20)	4.83	4.43	5.02	4.73	
π pop.	1.46 (15)	1.62	1.75	1.53	1.68	
N σ pop.	4.95 (20)	4.95	5.26	4.98	5.27	
π pop.	2.82 (15)	2.40	2.29	2.47	2.32	
C charge	0.24 (15)−	0.45−	0.17−	0.55− (0.39−[22b])	0.41−	0.36−
N charge	0.77 (10)−	0.34−	0.53−	0.45− (0.61−[22b])	0.59−	0.11−
cyanide π pop.	4.28 (15)	4.02	4.04	4	4	
cyanide σ pop.	9.75 (15)	9.78	9.69	10	10	
cyanide charge	1.0 (2)−	0.79−	0.70−	1.0−	1.0−	0.47−
metal-cyanide overlap pop.	0.15 (5)	0.19	0.26			
$q(L_\sigma \rightarrow M_\sigma)$	0.18 (5)	0.19 (6)	0.22 (1)			
$q(M_\pi \rightarrow L_\pi)$	0.06 (4)	0.0 (1)	0.02 (1)			
$q(L_\sigma \rightarrow L_\pi)$	0.23 (10)	0.0 (1)	0.01 (1)			

as would be expected if π(metal) $\rightarrow \pi^*$(ligand) back-bonding is occurring.

As previously,[22] we can interpret the σ-bonding 3d density and overlap with a simple MO, neglecting any π effects. We define the doubly degenerate bonding orbital wave functions as, for $Cr(CN)_6^{3-}$

$$\psi_b^1 = N_b^1[3d_{x^2-y^2} - \tfrac{1}{2}A_\sigma^{CN}(p_1 - p_2 + p_3 - p_4)]$$

$$\psi_b^2 = N_b^2[3d_{z^2} - A_\sigma^{CN}/\sqrt{12}(-p_1 - p_2 - p_3 - p_4 + 2p_5 + 2p_6)]$$

The N's are normalizing constants, p_1–p_6 are the ligand bonding orbitals, A_σ^{CN} is the covalence parameter, and we define S_σ^{CN} as $\langle 3d|p\rangle$. We have used the traditional octahedral coordinate system instead of the trigonal one (thus transforming $|e_g^+(\sigma)\rangle$ and $|e_g^-(\sigma)\rangle$ to $3d_{z^2}$ and $3d_{x^2-y^2}$) since there is no evidence of lower symmetry covalent effects. We define similar functions for $Co(NH_3)_6^{3+}$—$A_\sigma^{NH_3}$ and $S_\sigma^{NH_3}$. Use of the parameters for 3d σ population and overlap give respectively $A_\sigma^{CN} = 1.48$, $S_\sigma^{CN} = 0.12$ and $A_\sigma^{NH_3} = 1.28$, $S_\sigma^{NH_3} = 0.28$.

We can compare these values with those obtained for the Ni^{II}–NH_3, Ni^{II}–NO_2^- and Co^{II}–Cl^- bonds:[22] $A_\sigma^{NH_3} = 0.57$, $S_\sigma^{NH_3} = 0.08$; $A_\sigma^{NO_2} = 0.67$, $S_\sigma^{NO_2} = 0.10$; $A_\sigma^{Cl} = 0.15$, $S_\sigma^{Cl} = 0.15$.

In both the M(III) ions of the present case the covalence parameter, A, is substantially greater than for the M(II) ions and this is in complete accord with both theory and chemical experience. The Cr–CN bond seems to be marginally more covalent than the Co–NH_3 bond. Given the relative positions in the spectrochemical series, we expect M–CN bonds to be more covalent than M–NH_3 bonds, although more detailed analysis shows that charge and spectroscopic effects are not necessarily congruent.[25] This effect may be almost balanced by the greater covalence expected for the later transition metal, Co, relative to that of Cr earlier in the series. We have previously noted[5,22] a possible correlation between bonding strength and 3d orbital size. From Table VI we see a greater contraction of the Cr 3d orbitals than for Co, as this correlation would lead us to expect for the more strongly covalent bond. For $Cr(CN)_6$ the overlap parameters are similar to the values for M(II), as we would expect. For $Co(NH_3)_6$ the value of 0.28 for $S_\sigma^{NH_3}$ seems too large, unless there is considerable contribution of more diffuse orbitals to the bonding, which we do not observe.

(II) Ligand Region. If we use these covalence parameters and the model, we predict a charge transfer of 0.28 electron from the cyanide framework to the Cr atom and overlap regions, and 0.38 electron from the ammonia lone pair in relationship to the Co atom. Table VI shows 5.57 (15) σ valence electrons and 4.28 (15) π electrons in the cyanide group.

In Table VIII we show the partitioning between σ and π and C and N by our refinement and compare it with theoretical calculations for CN^-. While there is broad agreement, the differences are better discussed by reference to the Fourier difference maps (Figures 1a and 2a), the corresponding maps for NaCN·$2H_2O$,[20] and a theoretical calculation.[20,26] The agreement between theory and the data for cyanide in NaCN·$2H_2O$ is satisfactory.[20,21] Compared to these results we observed, in agreement, a large mid-bond density and rather smaller σ-lone-pair densities associated with N(1) and C(1). However, we also observe holes along the σ axis on either side of N(1) and C(1), indicating that, relative to the theoretical free atom, the σ-bonded atomic orbitals, $(sp)_1$ and $(sp)_2$, are depopulated in this region. Given the presence of the highly charged Cr(III) ion, even apart from any covalence effects, such a change is not surprising. We have chosen to analyze σ and π populations with a common radial dependence of electron density. To allow the σ and π radial dependences to differ would modify the populations—perhaps bringing them closer to the free-ion values of 10 and 4—but would be a gross overparameterization of our data.

The π-electron population of 4.28 (15) may show a slight excess over the value of 4.0 expected from simple considerations for the CN group. However, a more drastic discrepancy is the high π population on N(1) and its consequent depletion on C(1), and the inequality of the π_z and π_y populations, which removed the cylindrical symmetry. These effects may be of "intermolecular" origin and to some extent are in the direction expected for the C(1)–N(1)···H–N(2) hydrogen bonding.

For the ammonia molecule the $(sp^3)_1$-lone-pair hybrid on N(2) has 1.45 (4) electrons while the remaining three, directed at the hydrogen atoms, average 1.23. Taken with the hydrogen atoms, each N–H bond has close to the ideal population of 2.00 electrons, viz. 2.02. There is a loss (0.55 electron) from the nitrogen lone pair to the Co atom, as predicted by the simplest models of covalence in a complex ion, and the value is in fair conformity with that (0.38) which arose from our simple MO modeling. The valence charge distribution in the ammonia molecule resembles that found in $Ni(NH_3)_4(NO_2)_2$ in some detail.[5] There also the $(sp^3)_1$ hybrid has a distinctly higher population, 1.57 electrons, than have the other orbitals, which average 1.22 electrons, but again corresponding to the donation of about 25% of the lone pair to the metal atom. The total N–H valence population is close to the ideal, averaging 2.09 electrons. In $Ni(NH_3)_4(NO_2)_2$ the NH_3 molecule is coordinated fairly covalently to a metal atom and engages in some strong hydrogen bonding, so that the similarity in the results lends support to the X-ray method for detailed

(25) Figgis, B. N.; Reynolds, P. A. *J. Chem. Soc., Dalton Trans.*, in press.

(26) (a) Bonnaccorsi, R.; Petrolongo, C.; Scrocco, E.; Tomasi, J. *J. Chem. Phys.* **1968**, *48*, 1500. (b) Bonnaccorsi, R.; Petrolongo, C.; Scrocco, E.; Tomasi, J. *Chem. Phys. Lett.* **1969**, *3*, 473.

charge density analysis for coordination complexes.

(III) Parameterization of Charge Flows in the Hexacyanochromate(III) Ion. We define the charge flows and estimate them from the metal $3d_\sigma$ and $3d_\pi$ populations and cyanide σ and π populations: (i) *from* each cyanide σ system to the metal d_σ orbitals, $q(L_\sigma \rightarrow M_\sigma)$, i.e. σ bonding, 0.18 (5) e; (ii) *from* the metal d_π orbitals to each cyanide's π orbitals, $q(M_\pi \rightarrow L_\pi)$, i.e. π back-bonding, 0.06 (4) e; (iii) *from* the cyanide σ orbitals to the π orbitals, $q(L_\sigma \rightarrow L_\pi)$, i.e. ligand polarization, 0.23 (10) e.

It thus appears that σ charge transfer is larger than π, but surprisingly an even bigger effect may be the direct polarization of the cyanide ions. While we are used to the idea of the initially spherical metal ion being polarized by the ligands to give aspherical 3d densities, the corollary, which we observe here, is often ignored although the spectroscopic effects of ligand polarization are recognized.[27] In $Cr(CO)_6$ Rees and Mitschler[28] observed a similar polarization of the CO ligand but here the σ- and particularly π-bonding charge transfers are much larger. There is also theoretical doubt as to the contribution of π^*-type excited states by configurational interaction in the ground state of these molecules.[29] The difference observed between CN^- in $NaCN{\cdot}2H_2O$[21] (uncoordinated CN^-) and $Cr(CN)_6^{3-}$ (coordinated) is experimentally obvious: CN^- in the free state appears to have less π^* contribution than in the $Cr(CN)_6^{3-}$ ion. In addition the direct polarization $q(L_\sigma \rightarrow L_\pi)$ is much more significant than the polarization via metal 3d orbitals ($q(L_\sigma \rightarrow M_\sigma) + q(M_\pi \rightarrow L_\pi)$). We may thus be able to distinguish this "crystal field" polarization from a similar polarization caused by covalence, although the errors are sufficiently large that this conclusion needs to be supported by further experiment.

In these complexes, as in previous cases,[5,14,22] simple ligand field theory provides a first approximation in accounting for the metal–ligand bonding. However, the empirical parameters probably mask quantitative inadequacy. In the similar case of $Ni(NH_3)_4(NO_2)_2$ there was good internal consistency in the X-ray and the polarized neutron diffraction results taken separately. Only a comparison *between* these two sets of results provided evidence of a more complex situation. It will be valuable to compare our results for the $Cr(CN)_6$ ion with the projected spin density analysis. We may perhaps expect the greater covalence here to cause an even greater discrepancy.

(h) Theoretical Implications. The observations of σ donation of N and C lone pairs into Co or Cr 3d orbitals, π back-bonding, and CN^- polarization are attractive in terms of qualitative ideas of coordination chemistry, but at a more quantitative level these ideas present difficulty. Experimentally, the spectra,[1] magnetic susceptibility,[30] ESR,[30] and other physical measurements establish the ground terms of the Co and Cr atoms in the ions as $^1A_{1g}$ and $^4A_{2g}$, respectively, in the octahedral ligand field approximation. On the crystal field formalism these arise from the t_{2g}^6 and t_{2g}^3 d-orbital configurations. For our results, $3d^{6.65}$ for Co and $3d^{3.73}$ for Cr, the ground terms deduced in a crystal field model would not correspond at all well with $^1A_{1g}$ and $^4A_{2g}$.

An adequate description must include the covalence naturally, as is the case with modern theoretical treatments. Calculations on $Co(NH_3)_6^{3+}$, by ab initio molecular orbital methods, have been reported by Kalman and Richardson.[31] For $Cr(CN)_6^{3-}$ there have been a number of calculations, the latest being those of Sano et al. using ab initio[32,34] and $X\alpha$ methods,[33] in which they have also calculated for free cyanide ion for purposes of comparison. Selected electronic populations, both experimental and theoretical, are listed in Table VIII. Comparison of populations derived by decomposition of a single-crystal electron density in different ways for different calculations or experiments can only be semiquantitative. For example, the nitrogen charge in the free CN^- estimated by Milliken analysis can be unrealistic and it is better estimated by integration over the total electron density in the N region.[21] The preferred methods of comparison, calculated and experimental total electron densities or of structure factors, are not justified by the level of calculation available.

For $Co(NH_3)_6^{3+}$ the theory predicts[31] a $3d_\sigma$ population of 1.40 electrons by σ donation from ammonia a_1 orbitals, together with an unchanged $3d_\pi$ population of 6.00. We observe 1.08 (15) and 5.58 (20), respectively, in reasonable agreement.

In the case of $Cr(CN)_6^{3-}$ (Table VIII) the experimental and theoretical $3d_\sigma$ populations on Cr are in good agreement, as is the low 4s/4p population. The experimental $3d_\pi$ population is marginally lower than the theoretical values, while the overall metal charge agrees. In the cyanide ion the total σ populations agree, as do the Cr–C(1) overlap populations, but the π population is marginally higher than the theoretical. If we interpret these values in terms of $q(L_\sigma \rightarrow M_\sigma)$ and $q(M_\pi \rightarrow L_\pi)$, we see that theory and experiment are in excellent agreement over the σ donation and also agree that π back-bonding is much smaller, perhaps even negligible. The total cyanide charge and its partitioning between C(1) and N(1) are in reasonable agreement if we allow for the distortion of the ab initio populations caused by Mulliken population analysis. We observed 1.0 (2)–, 0.24 (15)–, and 0.77 (10)–, respectively, while $X\alpha$ gives 0.7–, 0.17–, and 0.53–, and we can estimate the ab initio (integrated) values as 0.79–, 0.29–, and 0.50–. However, there is a discrepancy between theory and experiment in the cyanide ion configuration. The most serious disagreement is the extra population on N(1) observed experimentally. The value of $q(L_\sigma \rightarrow L_\pi)$ implies that 0.23 (10) electron are removed from the σ system and are deposited in the cyanide π system, while the cyanide π system is itself polarized. This is a quantification of what is self-evident from comparison of the various experimental and theoretical density maps, but the valence-electron model does not account for the strong features in the CN region (Figure 2a). These features contrast strongly with both theory (free CN^-) and experiments on "free" cyanide ion in $NaCN{\cdot}2H_2O$.

This agreement leads us to suspect a $\sigma \rightarrow \pi$ polarization of the cyanide ion by the Cr(III) ion in our crystal. We have charge and spin density studies in progress on $Cs_2KCr(CN)_6$ to study whether the effect is a real, reproducible property of the free $Cr(CN)_6^{3-}$ ion.

Registry No. $[Co(NH_3)_5(H_2O)][Cr(CN)_6]$, 60897-44-1.

Supplementary Material Available: Listings of observed and calculated structure factors for the refinement PAA-A at 120 K and of anisotropic thermal parameters (Tables IIIB and VB) (27 pages). Ordering information is given on any current masthead page.

(27) Mason, S. F. *Structure Bonding (Berlin)* **1980**, *39*, 43.
(28) Rees, B.; Mitschler, A. *J. Am. Chem. Soc.* **1976**, *98*, 7918.
(29) Becker, P., unpublished results.
(30) Konig, E. "Landolt-Börnstein Physikalische und Chemische Tabellen"; Hellwege, K.-H., Ed.; Springer-Verlag: Berlin, 1966; Neue Serie II/2.
(31) Kalman, B. L.; Richardson, J. W. *J. Chem. Phys.* **1971**, *55*, 4443.
(32) Sano, M.; Kashiwagi, H.; Yamatera, H. *Inorg. Chem.* **1982**, *21*, 3837.
(33) Sano, M.; Adachi, H.; Yamatera, H. *Bull. Chem. Soc. Jpn.* **1981**, *54*, 2898.
(34) Sano, M.; Yamatera, H.; Hatano, Y. *Chem. Phys. Lett.* **1979**, *60*, 257.
(35) Leung, P. C.; Schultz, A. J.; Figgis, B. N. *Acta Crystallogr., Sect. C: Cryst. Struct. Commun.*, in press.